Ann. occup. Hyg., Vol. 49, No. 1, pp. 61–71, 2005

Published by Oxford University Press
doi:10.1093/annhyg/meh078

Applying Open-Path FTIR with Computed Tomography to Evaluate Personal Exposures. Part 1: Simulation Studies

CHANG-FU WU[1]*, MICHAEL G. YOST[1], RAM A. HASHMONAY[2], TIMOTHY V. LARSON[3] and STEVEN E. GUFFEY[4]

[1]Department of Environmental and Occupational Health Sciences, Box 357234, University of Washington, Seattle, WA 98195; [2]ARCADIS, PO Box 13109, Research Triangle Park, NC 27709; [3]Department of Civil and Environmental Engineering, Box 352700, University of Washington, Seattle, WA 98195; [4]Department of Industrial and Management Systems Engineering, West Virginia University, Morgantown, WV 26506, USA

Received 5 August 2003; in final form 19 August 2004; published online 13 December 2004

This paper presents the theoretical background and the numerical evaluation results obtained using computed tomography coupled with open-path Fourier transform infrared (CT-FTIR) measurements to estimate personal exposures. In this simulation study, we first tested the one-dimensional scenario with a five-beam segment geometry. A series of Gaussian plumes and the corresponding path-integrated concentrations (PICs) were simulated. The personal exposures were estimated as the average of the point estimates calculated from the workers' locations and the concentration profiles reconstructed from the Smooth Basis Function Minimization algorithm. It was found that the running-average PIC updating strategy has similar performance as the spline PIC updating strategy. However, the latter strategy gives delayed estimates of the workers' exposures since it requires additional measurements before and after the time period of interest. In the two-dimensional scenario, we simulated a series of single-mode bivariate Gaussian plumes with a nine-beam radial geometry. The average of the estimated exposures from the CT-FTIR approach was close to the average of the true exposures. The concordance correlation factors between the true and estimated exposures were reasonably good (between 0.50 and 0.58). This study demonstrated that the CT-FTIR approach is feasible for industrial hygiene monitoring.

Keywords: computed tomography; open-path FTIR; optical remote sensing; personal exposure; radial plume mapping

INTRODUCTION

In the field of industrial hygiene, personal exposures are usually evaluated using either sampling pumps with appropriate collecting media or passive sampling devices. The monitoring equipment is placed on the workers and air samples are collected for a full working shift; measurements are then compared with the 8 h time weighted average (TWA) exposure limits. However, in addition to the 8 h TWA standards, there are also concerns about short-term exposures. Currently, 25% of the compounds listed by the American Conference of Governmental Industrial Hygienists (ACGIH) have a short-term exposure limit (STEL) or ceiling value. Evaluations of STEL exposures are generally more difficult than evaluations of 8 h TWA exposures for several reasons. First, most personal sampling technologies (e.g. charcoal tube sampling) require minimum sample periods of hours, not minutes, for accurate laboratory analyses. Second, taking consecutive 15 min samples over a long period of time is labor intensive and interferes with normal working practices. Third, they generally require later analyses, making immediate feedback of results difficult or impossible. When acutely toxic agents are present, the time lag between sampling and analysis may be unacceptable. Although some modern real-time monitors may be used to evaluate the short-term exposure levels *in situ*, they only can monitor certain types of air

*Author to whom correspondence should be addressed.
Fax: +1-206-543-8123; e-mail: cfwu@u.washington.edu

contaminants. Each type of contaminant needs a specific type of detector. In other words, prior knowledge about the chemical properties of the existing gases or vapors is required, but is not always available.

To overcome some of these problems, we propose to use an optical remote sensing (ORS) technique to monitor personal exposures. More specifically, we emphasize the application of one ORS instrument: open-path Fourier transform infrared (OP-FTIR) spectroscopy (Sigrist, 1994). Before we explain this approach further, it is necessary to understand the reasons behind the current practice of using personal samplers for monitoring personal exposures. The 'personal sampling' concept was originated by Patterson (1939) and modified by Oldham and Roach (1952). It was argued that personal exposures could be very different from measurements taken in general, fixed areas (Perkins, 1997). The low correlations between the personal samples and area samples were usually attributed to a lack of understanding of spatial correlation between the area samples and the workers. However, modern technology has helped overcome this limitation. For example, the consumer-level global position system (GPS) can locate an object with an accuracy of a few meters. In general, as area monitors are less limited in their size and power requirements at the design stage, they can usually monitor multiple compounds and have faster response times and lower detection limits than personal monitors. If area monitors can be used to evaluate personal exposures, we can benefit from these advantages. Moreover, with multiple area monitors deployed in the working space, we can also identify the emission source of the air contaminant and then fix the release source. This kind of information is not typically available by simply collecting samples on workers. Therefore, it seems appropriate to re-evaluate the use of area monitors to monitor personal exposures.

OP-FTIR has some useful features for exposure assessments, such as identifying and quantifying mixtures of airborne compounds with low detection limits in real time (Levine *et al*., 1989; Yost *et al*., 1992). The data collected by OP-FTIR instruments are in the form of path-integrated concentration (PIC), usually presented in units of ppm-m. Using the PIC data of only one fixed beam path, one cannot tell if the contaminant is uniformly distributed along the path or highly concentrated in a small area. To make OP-FTIR feasible for assessing personal exposures, spatial resolution of the PIC data must be obtained (see detailed explanation in the next section).

For workers working at a fixed workstations, the bi-beam strategy described by Wu *et al*. (2003b) could be used to obtain the spatial resolution of the PIC data and then quantify the personal exposures. The bi-beam strategy combines a long beam and a short beam measurement to calculate the average concentration level of the segmented region. For the work practices of workers moving along a line space [one-dimensional (1D)] or moving around a two-dimensional (2D) plane, we propose to apply the CT-FTIR approach [computed tomography (CT) coupled with OP-FTIR measurement] to estimate personal exposures. CT provides numerical solutions for reconstructing the spatial concentration distribution from a set of PIC data (Yost *et al*., 1994). Most CT-FTIR studies to date have focused on the agreement between the CT reconstruction maps and the maps interpolated from point samples (Todd and Leith, 1990; Yost *et al*., 1992; Drescher *et al*., 1996; Samanta and Todd, 1996; Bhattacharyya and Todd, 1997; Park *et al*., 1997; Hashmonay *et al*., 1999; Wu *et al*., 1999; Farhat and Todd, 2000). However, for application to industrial hygiene, we need to know how well the CT-FTIR approach can monitor personal exposures. In other words, we want to know the correlations not only between the OP-FTIR measurements and area sampling but also between the OP-FTIR measurements and personal sampling. There have been few studies on the latter type of correlations (Yost *et al*., 1999; Ross and Todd, 2002; Wu *et al*., 2003b). In this paper, we develop the theory of applying CT-FTIR to estimate personal exposures and present results from our numerical simulation studies. The objective is to demonstrate the use of CT-FTIR to evaluate the 15 min TWA personal exposures. Although we could not simulate all real-world conditions, this type of simulation study provides valuable insights into the theory of the estimation approach, since various parameters can be controlled or adjusted to evaluate their effects. This is a cost-effective way to validate the system's performance before conducting more time- and cost-consuming chamber or field studies.

Theory development

In theory, by integrating a worker's exposure level at each location over time, we can obtain his or her cumulative exposure. The TWA concentration is the cumulative exposure divided by the total monitoring time, i.e.

$$C_{\text{avg}} = \frac{1}{T}\int_0^T C(t,x)\mathrm{d}t \qquad (1)$$

where T is the total monitoring time and $C(t, x)$ is the concentration at time t at location x. This sampling approach involves two major concepts. First, we need a concentration profile (or map) over space during the sampling period. This map can be obtained from the CT-FTIR reconstructions. Second, it is necessary to know the workers' positions in real time. This information may be obtained by applying the technique of motion tracking with image analysis. The motion tracking technique was described by Wu *et al*. (2004).

In principle, this description of exposures using a location-history and spatial concentration map should be equivalent to a conventional time series of exposures measured on a moving person. However, in practice, we do not know how errors in the spatial information will affect the exposure estimates or what temporal resolution is needed to achieve an equivalent integrated exposure estimate. To evaluate the performance of this new sampling approach, we conducted a series of numerical simulation studies on both 1D and 2D scenarios. Although applications are limited for the 1D scenarios, it serves as a basic model for understanding the more complex 2D scenarios.

METHODS

One-dimensional scenarios

Simulations of contaminant distributions and workers' locations. In the real world, a common observation is that the distribution of a contaminant at a certain time point is dependent on its distribution a short time period ago; i.e. concentration data in time are serially correlated. This kind of phenomenon is usually covered by time series analysis (Chatfield, 1996). In this study, we adopt a simple model, called the first-order autoregressive process, to simulate the time series data. The common form of this autoregressive process for the purpose exposure assessment is given by Francis *et al*. (1989):

$$(y_{t+1} - \mu) = \alpha(y_t - \mu) + \varepsilon_t \qquad (2)$$

where y_t and y_{t+1} are the plume's parameter (e.g. peak location) at time t and $t + 1$, μ is the expected average of the time series y, α (between 0 and 1) is the weighting factor for the past value, ε_t is a series of normally distributed random values with mean of 0 and standard deviation of $\sigma(1 - \alpha^2)^{0.5}$ and σ is the standard deviation of the time series y.

For the 1D scenarios, we simulated a series of Gaussian plumes with autocorrelated peak locations and fixed standard deviations. Using artificial Gaussian plumes allowed a direct comparison between the input test maps and the CT reconstruction maps. The probability density function of the Gaussian plumes at location x is (Fisher and Van Belle, 1993):

$$G(x;\mu,\sigma,h) = h \cdot \left(\sqrt{2\pi}\sigma\right)^{-1} \exp\left[-\frac{1}{2}\left(\frac{x-\mu}{\sigma}\right)^2\right] \qquad (3)$$

where μ is the peak location, σ is the standard deviation and h is the peak height. We also simulated a series of autocorrelated workers' locations with equation (2). One plume and one worker's location were simulated every second during a 15 min time period. Therefore, for each 15 min realization, we have 900 (15 min $\times$ 60 s/min) autocorrelated plumes and 900 autocorrelated workers' locations. Before the 15 min simulations, we allowed a 3 min 'warming period' to randomize and stabilize the time series data.

Two different test conditions were simulated, each consisting of 120 realizations. For the first test condition, the starting points of the warming period for the plumes' peak locations and workers' locations were both at the center of the 1D domain (2.5 m). The expected mean values were also 2.5 m. The weighting factor α was 0.95 (α_{plume}) for the plumes' peak locations and 0.98 (α_{worker}) for the workers' positions. The simulated plumes have a fixed standard deviation of 0.5 m. Figure 1 shows an example of a 15 min realization. The x-axis is the OP-FTIR's scanning beam path, the y-axis is the time in seconds, and the z-axis is the simulated concentrations. Each dot in this figure represents the worker's position at that time point. In the second test condition, we kept all the parameters that were used in the first test condition unchanged, except for α_{plume}, which was decreased from 0.95 to 0.82. This was used to test how well this system performed under a situation where the concentration fields changed more rapidly over time.

Beam geometry and PIC simulations. A five-beam geometry was tested in this study. Retroreflectors were placed at every meter along the 5 m long 1D scanning domain. Two factors were considered to determine the numbers of beam paths: spatial resolution and scanning time. It is commonly assumed that more beam paths are required to get higher spatial resolutions of the CT reconstruction maps. However, the time for OP-FTIR to scan a complete round over the monitoring areas increases in proportion to the numbers of beam paths, lowering the temporal resolution. Although the current five-beam geometry may not be the optimized arrangement, preliminary simulation studies showed that it could provide reasonably good CT reconstruction maps.

We assumed that the OP-FTIR required 10 s to scan each beam path. This simulated that our OP-FTIR instrument (Wu *et al*., 1999) acquired at least 15 spectra at 2 cm^{-1} spectral resolution during the 10 s period in order to have low noise levels in the final spectra. The OP-FTIR scanned sequentially from the nearest retroreflector (at 1 m) to the farthest retroreflector (at 5 m), repeating this sequence for 15 min. With five beam paths, the OP-FTIR scanned the same beam path every 50 s. We simulated the observed PIC data by averaging the integrations of the length of a ray over the Gaussian plume's density function during the 10 s measurement period (Wu *et al*., 2003a).

CT reconstruction. The Smooth Basis Function Minimization (SBFM) algorithm was applied to perform the CT reconstruction (Drescher *et al*., 1997; Hashmonay *et al*., 1999; Tsai *et al*., 2001). SBFM fits smooth functions with a limited number of parameters to satisfy the input ray integrals. The basis

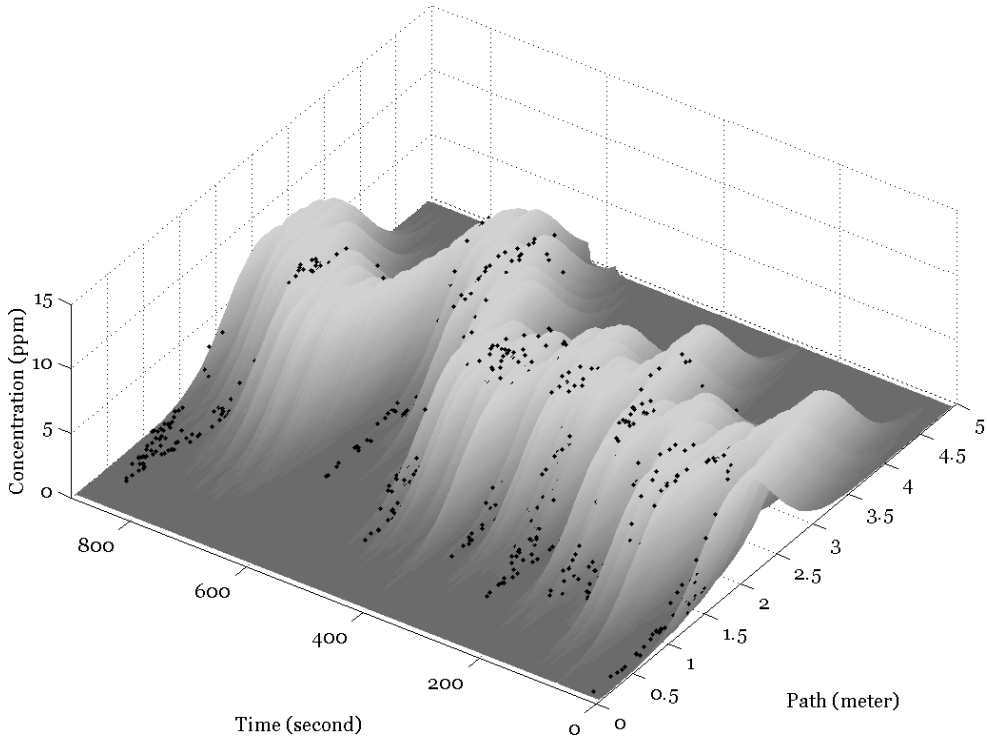

Fig. 1. An example of the simulated Gaussian plumes and the worker's locations in the 1D scenarios. *x*-Axis is the OP-FTIR's scanning 1D domain; *y*-axis is the time; and *z*-axis is the simulated concentration levels. The dots represent the worker's locations.

function in this study was the one-mode Gaussian function with three parameters: peak location, standard deviation and peak height. The error function for minimization was the sum of squared errors (SSE) between the observed and predicted PIC. For 1D SBFM, the predicted PIC is defined as follows:

$$\mathrm{PIC}_{\mathrm{predicted},i}(p_{jk}) = \sum_{k} \int_{o}^{L_i} G_k(x; p_{jk})\,\mathrm{d}x \quad (4)$$

where j is the parameter number index and k is the basis function number index; L_i is the ith ray path length and p_{jk} is the jth parameter of the kth basis function; G_k is the kth basis function. In this study, $k = 1$ (one Gaussian), i ranged from 1 to 5 (five rays) and j ranged from 1 to 3 (three parameters for one Gaussian distribution). The algorithm to minimize the SSE is adopted from the Matlab software's *lsqnonlin*() function (MathWorks, Inc., Natick, MA), which is designed for solving nonlinear least-squares problems.

For most of the minimization algorithms, it is important to provide a good first guess as an initial starting searching point. We applied a Monte Carlo technique to find the first guess. A total of 400 trials were generated before the first SBFM reconstruction. During each trial, a set of Gaussian parameters was randomly sampled from a uniformly distributed probability range ($1\ \mathrm{m} < \mu < 4\ \mathrm{m}$; $0.2\ \mathrm{m} < \sigma < 2.2\ \mathrm{m}$; $5\ \mathrm{ppm} < h < 15\ \mathrm{ppm}$). Each set of Gaussian parameters was used to calculate the predicted PICs from equation (4) and the corresponding SSE values. The least SSE value among the 400 trials was used as the first guess of the minimization algorithms for the first reconstruction. For the following reconstructions, the resulting parameters found by the minimization algorithms from the previous round were used as the first guess for the next round. If the minimization algorithms found an unrealistically narrow plume (i.e. SD < 0.2 m) or did not converge to a solution, a new first guess was obtained again from the Monte Carlo technique.

To obtain one reconstruction of a Gaussian plume, we employed five observed PICs (one PIC from each of the five rays). Three different PIC updating strategies were evaluated here. (i) Running-average PIC (PICrun): Every 10 s, the oldest PIC was updated with the latest PIC and the other four PICs were unchanged. Therefore, the five PICs were updated completely every 50 s. This is the most straightforward way to update the PIC information. (ii) Spline PIC (PICsp): For each ray, we splined (De Boor, 1978; Chatfield, 1996) the PICs to interpolate the observed PICs. In order to have better estimates at the beginning and at the end of the 15 min periods, we included the PIC values 3 min before and after the 15 min periods into the interpolation process. (iii) Concurrent PIC (PICcon): In this updating strategy, we assumed that all five rays could be updated every 10 s. Although this was not a practical

assumption, these PICs represented the ideal PICs and could be used to confirm the performance of the beam geometry and minimization algorithms.

Calculate 15 min TWA. The TWA exposure is a function of the concentration profiles and the workers' locations. Equation (1) can be rewritten as:

$$C_{\text{avg}} = \frac{1}{T}\sum_{t=1}^{T} G_t(x_t, \mu_t, \sigma_t, h_t) \qquad (5)$$

where T is the total monitoring time; G_t is the spatial concentration distribution function of the reconstructed Gaussian plume with peak location μ_t, standard deviation σ_t and peak height h_t at time t; x_t is the worker's location. In this study, since T was 900 s (=15 min) and the CT-FTIR reconstructed one plume every 10 s, we averaged 90 (=900/10) G_t values from 90 sets of reconstructed μ_t, σ_t and h_t values to get the estimated C_{avg}. The true C_{avg} can be calculated by averaging 900 G_t values from 900 sets of input μ_t, σ_t and h_t values.

One important issue here is how to incorporate the information about the workers' locations into equation (5). The CT reconstruction can only be performed every 10 s, but the workers' locations can be obtained every 1 s. Three different updating strategies were evaluated here. (i) Point location (Wpoint), which uses the worker's location at the last second during the latest reconstruction as the x_t. (ii) Ten seconds average (W10sec), which uses the average of the worker's locations during the past 10 s of the latest reconstruction as the x_t. (iii) Fifty seconds average (W50sec), which uses the average of the worker's locations during the past 50 s of the latest reconstruction as the x_t.

The concordance correlation factor (CCF_{TWA}) (Fisher and Van Belle, 1993; Hashmonay *et al*., 1999) between the true and estimated 15 min TWA values is chosen as a summary measure to represent the quality of the CT-FTIR estimation results. The CCF is similar to the Pearson correlation coefficient with adjustment for location and scale shifts. The CCF values are bounded between −1 and 1 and in this context reflect the overall accuracy and precision of the data.

Two-dimensional scenarios

Synthetic data and beam geometry. For the 2D scenarios, a series of bivariate Gaussian plumes were simulated over a rectangular spatial domain of 4 × 4 m. Each bivariate Gaussian is described by six parameters: the peak location (μ_x, μ_y), two standard deviations (σ_x, σ_y), the peak height and the correlation coefficient (ρ) (Hutchinson and Lai, 1991). The probability density function of the bivariate Gaussian is transformed from the Cartesian coordinate system (x, y) into the polar coordinates (L, θ):

$$G(L,\theta;\rho) = \left(2\pi\sqrt{1-\rho^2}\right)^{-1} \exp\left\{-\frac{1}{2(1-\rho^2)}\left[(L\cos\theta)^2 - 2\rho(L\cos\theta)(L\sin\theta) + (L\sin\theta)^2\right]\right\} \qquad (6)$$

where the peak location parameters (μ_x, μ_y) and standard deviation parameters (σ_x, σ_y) are introduced by replacing $L\cos\theta$ and $L\sin\theta$ with $(L\cos\theta - \mu_x)/\sigma_x$ and $(L\sin\theta - \mu_y)/\sigma_y$, respectively. The simulated Gaussian plumes had autocorrelated μ_x and μ_y with fixed σ_x and σ_y [equation (2)]. It was assumed that there was no correlation between the μ_x and μ_y. Workers were also simulated to walk around the same 2D spatial domain with autocorrelated x and y coordinates.

Two test conditions were simulated, each consisting of fifty 15 min realizations. In the first test condition, the α_{plume} was 0.95 and α_{worker} was 0.98, similar to the parameters used in the first test condition in the 1D scenarios. The bivariate Gaussian plumes had an expected peak location at $x = 2$ and $y = 0$ in the 2D scanning domain. The σ_x and σ_y were fixed values of 1. Figure 2 shows an example of the plumes' peak locations and workers' locations during one 20-s time period. The dark and light lines represent the plume's peak locations and worker's locations, respectively, from time t to $t + 19$. The grayscale bar shows the grayscale representations of the plumes' concentration levels at time $t + 19$. In the second test condition, the σ_x and σ_y values decreased to 0.5 to simulate a narrow plume.

The radial beam geometry applied in this study had nine beam paths. The angle between each ray was 6° and the end of each ray was approximately at the center of each grid (Fig. 3). It consisted of four long beam paths, three intermediate beam paths and two short beam paths. As found by Wu *et al*. (1999), segmenting information is important to the radial geometry. The proposed geometry in this study was designed to have more segmenting information in the region that was farther from the OP-FTIR. The high ray density near the OP-FTIR should compensate for the lack of segmenting information in the region near the instrument. Since this geometry did not cover the upper-left and lower-left corner of this spatial domain, we did not expect that the CT algorithm could reconstruct well in these two regions. Only a few simulated plumes had peak locations in these regions. A scanning geometry consisting of more beam paths could cover a wider area, but again there is a trade-off between the temporal and spatial resolution.

As in the 1D scenarios, we assumed that OP-FTIR required 10 s to scan each beam path. It scanned from 1 to ray 9 sequentially and came back to ray 1,

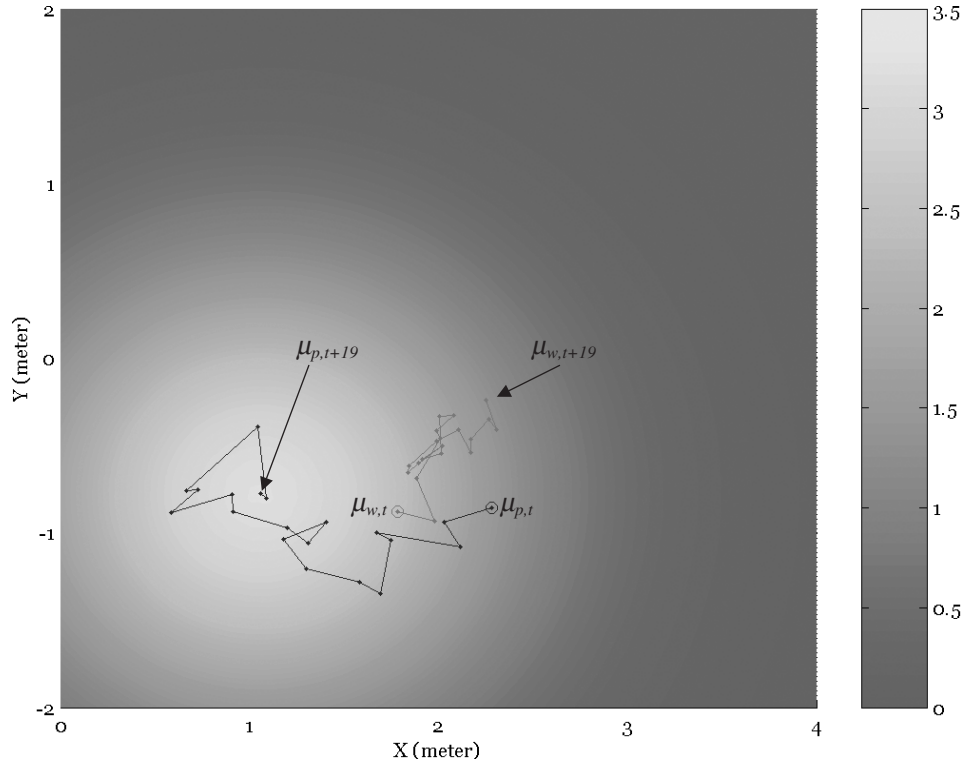

Fig. 2. An example of the simulated Gaussian plumes in the 2D scenarios during a 20 s time period. The dark line shows the plume's peak locations from time t ($\mu_{p,t}$) to $t + 19$ ($\mu_{p,t+19}$). The light line shows the worker's locations from time t ($\mu_{w,t}$) to $t + 19$ ($\mu_{w,t+19}$). The grayscale bar shows the grayscale representations of the plumes' concentration levels at time $t + 19$.

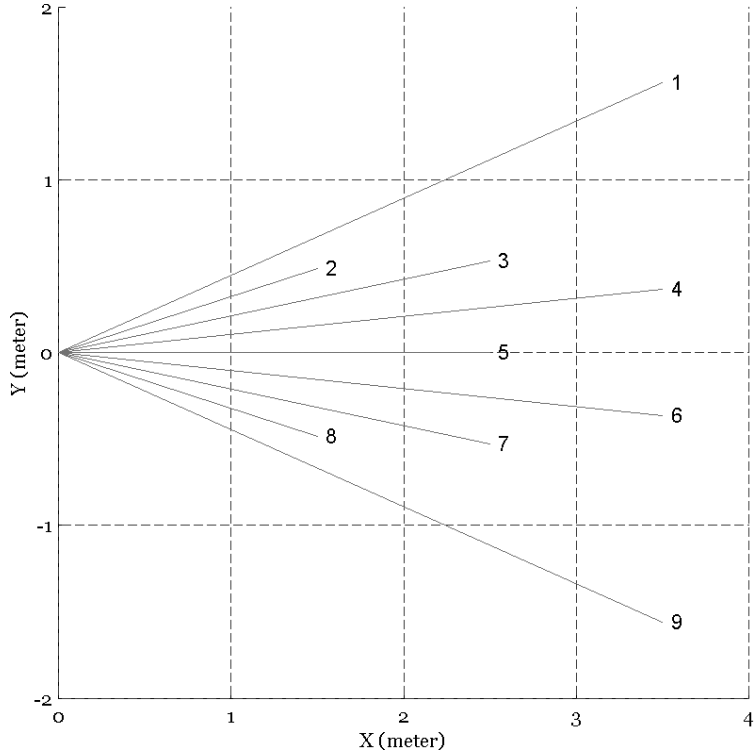

Fig. 3. The beam geometry of the OP-FTIR in the 2D scenarios. The OP-FTIR is located at (0, 0). The number at the end of each beam path is the beam ID.

repeating the same sequence for 15 min. The time interval for the OP-FTIR to scan the same beam path again increased to 90 s, compared with 50 s in the 1D scenarios. We simulated the observed PIC by averaging the integration of the length of a ray over the bivariate Gaussian plume's density function during the 10 s measurement period.

CT reconstruction and calculated 15 min TWA. The basis function applied in the SBFM algorithm in the 2D scenarios was a one-mode bivariate Gaussian function. The predicted PIC in the SSE function is defined as follows (Hashmonay and Yost, 1999):

$$\mathrm{PIC}_{\mathrm{predicted},i}(p_{jk}) = \sum_k \int_0^{L_i} G_k(r, \theta_i, p_{jk})\,\mathrm{d}r \quad (7)$$

where j is the parameter number index and k is the basis function number index; L_i is the ith ray path length and p_{jk} is the jth parameter of the kth basis function; $G_k(r, \theta_i, p_{jk})$ is the kth basis function in polar coordinates r and θ. In this study, $k = 1$ (one bivariate Gaussian), i ranged from 1 to 9 (nine rays) and j ranged from 1 to 6 (six parameters for one Gaussian distribution). The procedures of minimizing the SSE functions and to calculating the 15 min TWA were similar to the procedures used in the 1D scenarios.

In addition to evaluating the 15 min TWA values, we also assessed the performance of the SBFM reconstruction algorithm on a mapping basis for the 2D scenario. The area where the workers walked around was overlapped with an 8×8 grid system. Every 10 s, the Gaussian parameter vector p [equation (7)] obtained from the SBFM algorithm was applied with the one-mode bivariate Gaussian density function to calculate a reconstructed map based on the above grid system. The corresponding true map during the same 10 s period was the mean map of the ten 1 s maps calculated from the input Gaussian parameter vectors. Each realization produced 90 pairs of true and reconstructed maps. We calculated the CCF value (called $\mathrm{CCF}_{\mathrm{CT}}$) for each pair of maps. The mean of the 90 $\mathrm{CCF}_{\mathrm{CT}}$ values (called $\overline{\mathrm{CCF}}_{\mathrm{CT}}$) was used to determine the agreement between the true and reconstructed maps for each realization with a 10 s temporal resolution. We also calculated the CCF value between the mean maps of the 90 true maps and the 90 reconstructed maps (called $\mathrm{CCF}_{\mathrm{CTMean}}$). The $\mathrm{CCF}_{\mathrm{CTMean}}$ represented the time-weighted agreement between the true and reconstructed maps for each realization.

RESULTS AND DISCUSSION

One-dimensional scenarios

Figure 4a shows the results under the first test condition with different estimation strategies. The dotted line represents the average of the true 15 min TWA values from the 120 realizations. The closed diamonds show the average values with 1 SD of the estimated 15 min TWA values. The asterisks represent the $\mathrm{CCF}_{\mathrm{TWA}}$ values. The use of the PICcon updating strategy provides the best estimation with $\mathrm{CCF}_{\mathrm{TWA}}$ values close to 1. This confirms that our beam geometry and optimization procedures perform reasonably well under ideal conditions, although the PICcon cannot be obtained with our OP-FTIR instrument. Using the workers' 50 s averaged positions (W50sec) with either PICrun or PICsp produced biased estimates and relatively low $\mathrm{CCF}_{\mathrm{TWA}}$ values. As for the other estimation strategies, it is hard to determine which method performs best. The remaining four methods all have good $\mathrm{CCF}_{\mathrm{TWA}}$ values between 0.81 and 0.86. Further sensitivity analysis was later applied to the four candidates (Wpoint&PICrun; Wpoint&PICsp; W10sec&PICrun; W10sec&PICsp) to find the best method.

Figure 4b shows the results under the second test condition, where the concentration fields changed more rapidly over time, compared with the first test condition. Again, using the 50 s averaged workers' locations give biased estimates with lower $\mathrm{CCF}_{\mathrm{TWA}}$ values. The $\mathrm{CCF}_{\mathrm{TWA}}$ values for the four candidates decrease slightly but are still >0.80. This suggests that the proposed CT-FTIR approach works reasonably well under both rapidly and slowly changing conditions.

It does not seem reasonable intuitively that the W50sec updating strategy should offer poorer results than either Wpoint or W10sec, given that the PICrun updates completely every 50 s. We offer the following explanations for this discrepancy. The W50sec and W10sec strategies represented the average values of the workers' locations during the most recent 50 s and 10 s periods, respectively. Each location was equally weighted. However, PICrun updated only one input PIC every 10 s and the updated PIC covered only some part(s) of the plumes. This means that each input PIC might not be weighted equally when we reconstructed the concentration maps to represent the true average plume. Our results suggest that the PICrun may be more representative of the average plume in the past 10 s than the average plume over the past 50 s. This could explain why the W10sec performs better than the W50sec updating strategy.

The sensitivity analysis was first conducted on parameters for the workers' locations. Different noise levels were added on the simulated workers' locations for each of the 120 realizations under the first testing condition. The estimated 15 min TWA values were recalculated. Figure 5a shows that the strategies based on Wpoint are sensitive to added noise. When the noise levels are approximately >20%, the $\mathrm{CCF}_{\mathrm{TWA}}$ values drop quickly. This is the same for both reconstructions updated using the PICrun or PICsp strategy. Conversely, the strategies

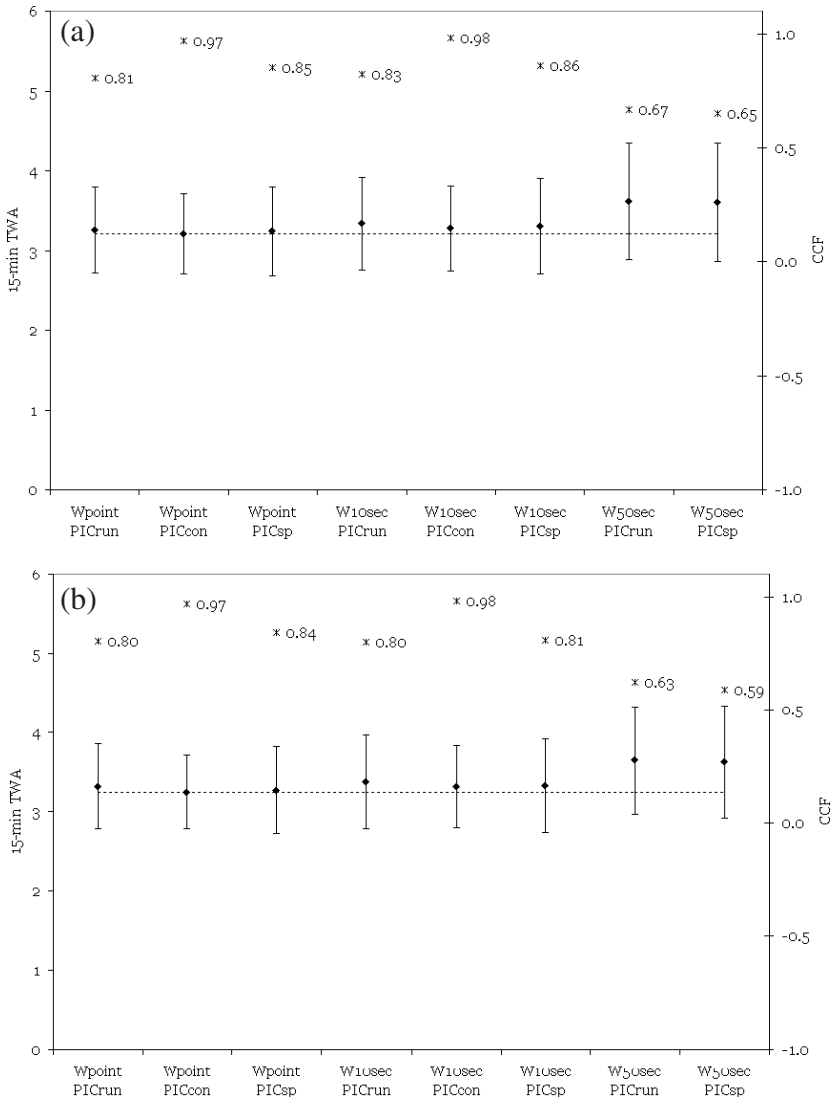

Fig. 4. Results from the 1D scenarios. The dotted line represents the average of the true 15 min TWA values from the 120 realizations. The closed diamonds show the average values with 1 SD of the estimated 15 min TWA values. The asterisks represent CCF_{TWA} values. (a) $\alpha_{plume} = 0.95$; $\alpha_{worker} = 0.98$; (b) $\alpha_{plume} = 0.82$; $\alpha_{worker} = 0.98$.

that update the workers' locations with W10sec are less sensitive to noise. The CCF_{TWA} values change little, even at high noise levels, regardless of the PIC updating strategies. This is understandable, because some of the errors were smoothed out during the averaging process.

A sensitivity analysis was also conducted on parameters of the observed PIC. Figure 5b summarizes these results. Generally, all the CCF_{TWA} values from PICrun and PICsp have a decreasing trend. With the same updating strategies for the workers' locations, there is not much difference between applying the PICrun and PICsp at different noise levels, in terms of the CCF_{TWA} values. However, calculating PICsp required additional measurements before and after the time period of interest to stabilize the interpolation process. This means that we will always get delayed estimates of the workers' exposures when applying PICsp, which makes PICrun the preferable updating strategy.

Two-dimensional scenarios

From the 1D scenarios, we determined that we should use the updating strategy of applying W10sec and PICrun. Therefore, we focused on this strategy in the 2D scenarios. For wide plumes (i.e. $\sigma_x = \sigma_y = 1$), Fig. 6a shows that the CCF_{TWA} value from PICcon is very close to 1. This confirms that our beam geometry and optimization algorithms work well. The CCF_{TWA} values from PICrun (=0.6) in the 2D scenarios are smaller than the CCF_{TWA} values (>0.8)

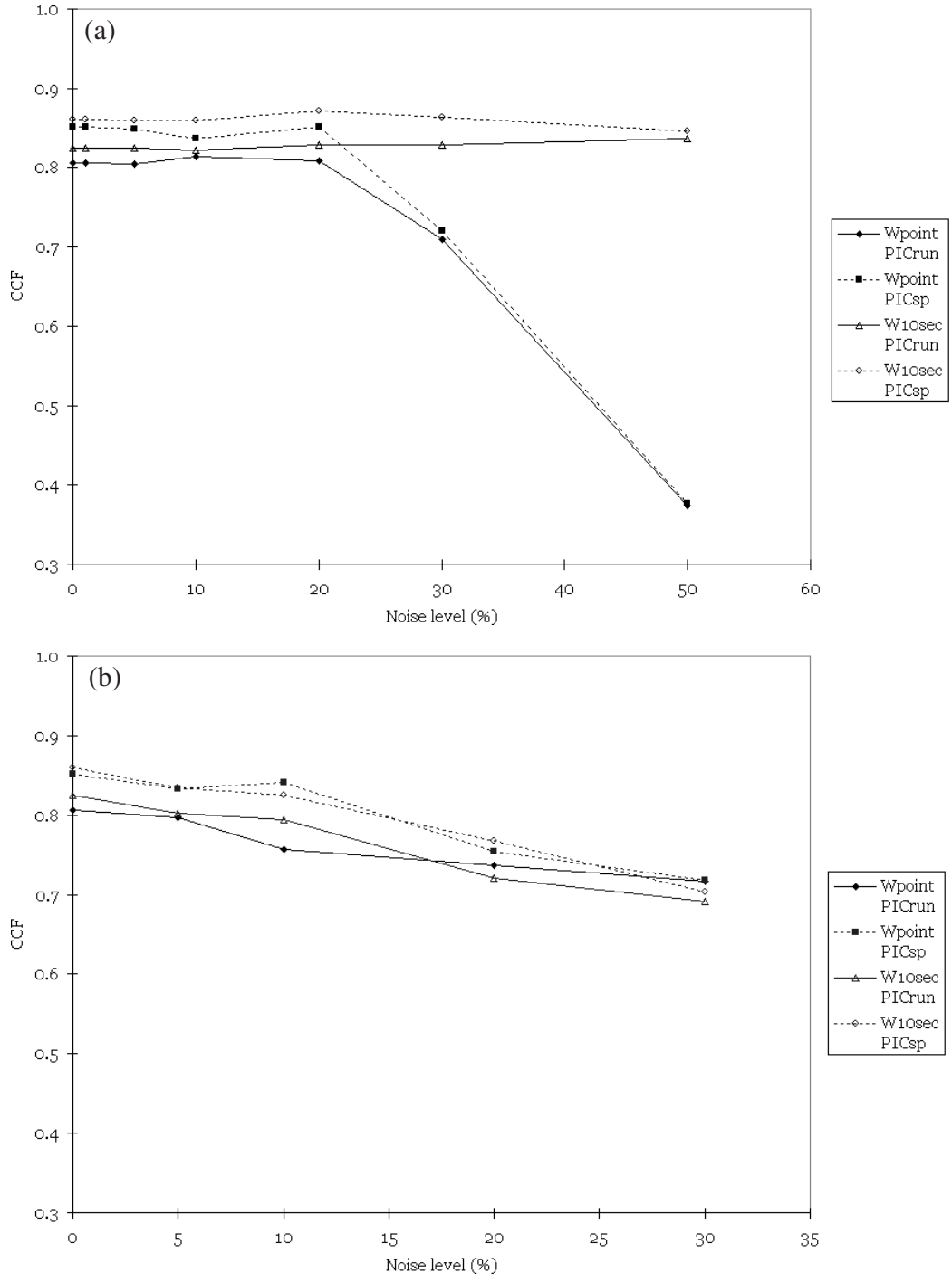

Fig. 5. Results from the sensitivity analysis in the 1D scenarios. Sensitivity of (a) the workers' locations and (b) the input PICs.

in the 1D scenarios. This is mainly because we kept α_{plume} and α_{worker} the same, but increased the scanning time for a complete round from 50 s in the 1D scenarios to 90 s in the 2D scenarios. However, the CCF_{TWA} values of 0.6 still represent reasonably good agreement between the true and estimated 15 min TWA values, and are within the range of experimental validation for CT-FTIR (Wu *et al*., 1999). For the 50 realizations, the average of the estimated 15 min TWA are close to the average of the true 15 min TWA.

In Fig. 6c, we decreased the σ_x and σ_y values to 0.5 to simulate narrower plumes. Again, the CCF_{TWA} value from PICcon is very close to 1, confirming the performance of the beam geometry and optimization algorithms. From previous studies (Hashmonay

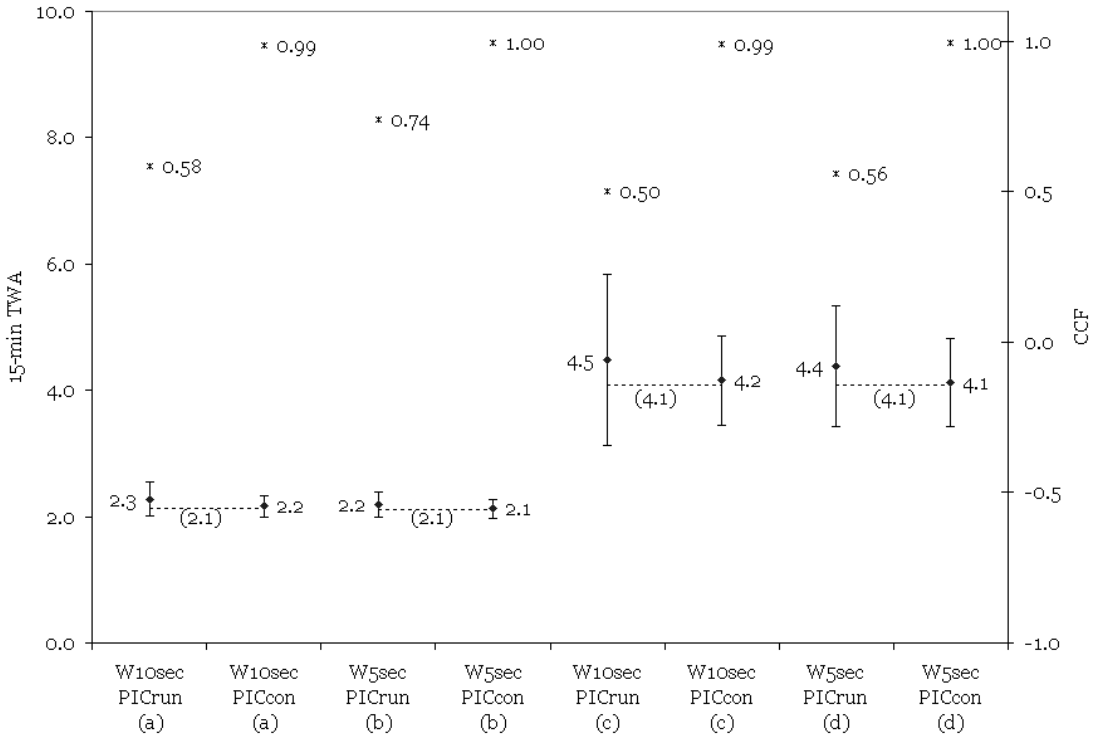

Fig. 6. Results from the 2D scenarios. The dotted line represents the average of the true 15 min TWA values from the 50 realizations. The closed diamonds show the average values with 1 SD of the estimated 15 min TWA values. The asterisks represent CCF_{TWA} values. (a) $\sigma_x = \sigma_y = 1$. The scanning time for each ray is 10 s. (b) $\sigma_x = \sigma_y = 1$. The scanning time for each ray is 5 s. (c) $\sigma_x = \sigma_y = 0.5$. The scanning time for each ray is 10 s. (d) $\sigma_x = \sigma_y = 0.5$. The scanning time for each ray is 5 s.

et al., 1999; Wu *et al*., 1999), we know that it is more difficult to reconstruct a narrow plume than a wide plume, given a radial beam geometry. The quality of the reconstructed map is a function of the beam density in the scanning domain. Therefore, it is not surprising to see that the CCF_{TWA} values from PICrun were smaller in Fig. 6c than in Fig. 6a.

One way to increase the agreement between the estimated and true 15 min TWA values is to decrease the time-scale difference between the plumes and the OP-FTIR's scanning time. Figure 6(b) and (d) shows the results for wide and narrow plumes, respectively, from the assumption that the OP-FTIR scanned each ray for 5 s. This reduces the time to scan a complete round to 45 s. The worker's location was also calculated as the average location during the past 5 s (W5sec). The CCF_{TWA} value increases from 0.58 in (a) to 0.74 in (b) and 0.50 in (c) to 0.56 in (d). Our OP-FTIR instrument can acquire approximately eight spectra during this 5 s scanning time. The disadvantage of decreasing the scanning time for each ray is that the collected spectra may contain more noise. Adding 7% noise to PICrun decreased the CCF_{TWA} to 0.63 and 0.52 for scenarios in Fig. 6(b) and (d), respectively. It is still larger than the corresponding CCF_{TWA} values if we assume the scanning time for each ray to be 10 s [Fig. 6(a) and (c)]. The 7% noise was a typical level for our OP-FTIR with eight scans for measuring carbon monoxide, which was used later as a tracer gas in a series of chamber experiments (Wu *et al*., 2004).

The mean $\overline{CCF}_{CT}$ with PICrun updating strategy for conditions (a), (b), (c) and (d) in Fig. 6 was 0.56, 0.61, 0.41 and 0.44, respectively. The mean CCF_{CTMean} with PICrun updating strategy for conditions (a), (b), (c) and (d) was 0.95, 0.98, 0.85 and 0.87, respectively. For each condition, the CCF_{TWA} lies between the mean $\overline{CCF}_{CT}$ and the mean CCF_{CTMean}. The reason for the CCF_{TWA} being larger than the mean $\overline{CCF}_{CT}$ is that the former measure was based on a single point comparison on the map while the latter measure compared the whole map (8×8 points). Although CCF_{CTMean} is also a measure based on the whole map, it is larger than the CCF_{TWA}. This is because the CCF_{CTmean} represents the overall fit during the 15 min period, where some of the errors are smoothed out by the time-averaging process. Since the CCF_{TWA} and the $\overline{CCF}_{CT}$ were based on the same temporal resolution, it was not surprising to see that the CCF_{TWA} was more similar to the $\overline{CCF}_{CT}$ than to the CCF_{CTMean}.

In real workplaces, workers do not move continuously, but stop at workstations to perform certain jobs. These conditions were not simulated here. From previous studies, we know that the quality of the reconstruction maps is not uniformly distributed

over the beam geometry. Some regions have good reconstructions while others do not. Therefore, the locations of the workstations and the time that the workers spend at the workstations will affect our ability to accurately estimate personal exposures. To make the CT-FTIR approach more practical and attractive, more simulation studies focusing on these different scenarios will be needed.

CONCLUSIONS

Using computer simulation data, we demonstrate that it is feasible to use the CT-FTIR approach to evaluate personal exposures, in terms of the 15 min TWA. Generally, the averages of the estimated 15 min TWA are close to the true 15 min TWA, i.e. the bias from the estimation method is small. The CCF between the estimated and true values depends on the simulation conditions. When we have a relatively wide plume and slowly changing conditions, the CCF_{TWA} values are high. Conversely, the CCF_{TWA} values are small when the plume is narrow with rapidly changing conditions. The high CCF_{TWA} (>0.99) from the PICcon updating strategy suggests that the performance of our approach was not limited by the SBFM algorithm, but mainly by the time required to scan each retroreflector. If we had an instrument that could scan all the retroreflectors simultaneously, we could significantly improve the $\overline{CCF}_{CT}$ and thus the CCF_{TWA} from the PICrun updating strategy.

Acknowledgements—We thank Ms. Kathy Hall for her assistance in editing the manuscript. This research was partially supported by the National Institute for Occupational and Safety Health (NIOSH) grant RO1OH02660. This does not constitute an endorsement of the views expressed in this article by NIOSH.

REFERENCES

Bhattacharyya R, Todd LA. (1997) Spatial and temporal visualization of gases and vapours in air using computed tomography. Numerical studies. Ann Occup Hyg; 41: 105–22.

Chatfield C. (1996) The analysis of time series: an introduction. London; New York: Chapman & Hall. ISBN 0412716402.

De Boor C. (1978) A practical guide to splines. New York: Springer-Verlag. ISBN 0387903569.

Drescher AC, Gadgil AJ, Price PN *et al*. (1996) Novel approach for tomographic reconstruction of gas concentration distributions in air: use of smooth basis functions and simulated annealing. Atmos Environ; 30: 929–40.

Drescher AC, Park DY, Yost MG *et al*. (1997) Stationary and time-dependent indoor tracer-gas concentration profiles measured by OP-FTIR remote sensing and SBFM-computed tomography. Atmos Environ; 31: 727–40.

Farhat SK, Todd LA. (2000) Evaluation of open-path FTIR spectrometers for monitoring multiple chemicals in air. Appl Occup Environ Hyg; 15: 911–23.

Fisher L, Van Belle G. (1993) Biostatistics: a methodology for the health sciences. New York: Wiley. ISBN 0471584657.

Francis M, Selvin S, Spear R *et al*. (1989) The effect of autocorrelation on the estimation of workers' daily exposures. Am Ind Hyg Assoc J; 50: 37–43.

Hashmonay RA, Yost MG. (1999) Innovative approach for estimating fugitive gaseous fluxes using computed tomography and remote optical sensing techniques. J Air Waste Manage Assoc; 49: 966–72.

Hashmonay RA, Yost MG, Wu CF. (1999) Computed tomography of air pollutants using radial scanning path-integrated optical remote sensing. Atmos Environ; 33: 267–74.

Hutchinson TP, Lai CD. (1991) The engineering statistician's guide to continuous bivariate distributions. Adelaide, SA: Rumsby Scientific Publishing ISBN 0646024132.

Levine SP, Ying LS, Strang CR *et al*. (1989) Advantages and disadvantages in the use of fourier transform infrared (FTIR) and filter infrared (FIT) spectrometers for monitoring airborne gases and vapors of industrial hygiene concern. Appl Ind Hyg; 4: 180.

Oldham PD, Roach SA. (1952) A sampling procedure for measuring industrial dust exposure. Br J Ind Med; 10: 227.

Park DY, Yost MG, Levine SP. (1997) Evaluation of virtual source beam configurations for rapid tomographic reconstruction of gas and vapor concentrations in workplaces. J Air Waste Manage Assoc; 47: 582–91.

Patterson HS. (1939) Bull Insn Min Metall; 417.

Perkins JL. (1997) Modern industrial hygiene. New York: Van Nostrand Reinhold. ISBN 0442021054.

Ross KR, Todd LA. (2002) Field evaluation of a transportable open-path FTIR spectrometer for real-time air monitoring. Appl Occup Environ Hyg; 17: 131–43.

Samanta A, Todd LA. (1996) Mapping air contaminants indoors using a prototype computed tomography system. Ann Occup Hyg; 40: 675–91.

Sigrist MW. (1994) Air monitoring by spectroscopic techniques. New York: Wiley. ISBN 0471558753.

Todd L, Leith D. (1990) Remote-sensing and computed-tomography in industrial-hygiene. Am Ind Hyg Assoc J; 51: 224–33.

Tsai MY, Yost MG, Wu CF *et al*. (2001) Line profile reconstruction: validation and comparison of reconstruction methods. Atmos Environ; 35: 4791–9.

Wu CF, Yost MG, Hashmonay RA *et al*. (2004) Applying open-path FTIR with computed tomography to evaluate personal exposures. Part 2: experimental studies. Ann Occup Hyg; in press.

Wu CF, Yost MG, Hashmonay RA *et al*. (2003a) Path concentration profile reconstruction of optical remote sensing measurements using polynomial curve fitting procedures. Atmos Environ; 37: 1879–88.

Wu CF, Yost MG, Hashmonay RA *et al*. (1999) Experimental evaluation of a radial beam geometry for mapping air pollutants using optical remote sensing and computed tomography. Atmos Environ; 33: 4709–16.

Wu CF, Yost MG, Varr J *et al*. (2003b) Applying open-path FTIR with a bi-beam strategy to evaluate personal exposure in indoor environments: Experimental results of a validation study. AIHA Journal; 64: 181–8.

Yost MG, Gadgil AJ, Drescher AC *et al*. (1994) Imaging indoor tracer-gas concentrations with computed tomography: experimental results with a remote sensing FTIR system. Am Ind Hyg Assoc J; 55: 395–402.

Yost MG, Hashmonay RA, Zhou Y *et al*. (1999) Estimating maximum concentrations for open path monitoring along a fixed beam path. J Air Waste Manage Assoc; 49: 424–33.

Yost MG, Xiao HK, Spear RC *et al*. (1992) Comparative testing of an FTIR remote optical sensor with area samplers in a controlled ventilation chamber. Am Ind Hyg Assoc J; 53: 611–16.